Erschienen in: Journal of Applied Physics ; 80 (1996), 2. - S. 1226-1232
http://dx.doi.org/10.1063/1.363731

Low-voltage electrochromic device for photovoltaic-powered smart windows

C. Bechinger,[a] J. N. Bullock, J.-G. Zhang, C. E. Tracy, D. K. Benson, S. K. Deb, and H. M. Branz
National Renewable Energy Laboratory, 1617 Cole Boulevard, Golden, Colorado 80401

(Received 20 October 1995; accepted for publication 11 April 1996)

We report the properties of an all-solid-state electrochromic (EC) device that can be switched over a useful range of optical transmissions with voltages below 1 V. This switching voltage is smaller than required by other solid-state EC devices reported to date. We attribute the lower-than-normal switching voltage to the use of a thermally evaporated MgF_2 thin film as the lithium ion conducting layer. Electrochemical impedance spectroscopy studies show that high lithium ion conductivity and low interfacial barriers for lithium exchange with the adjacent electrochromic and ion storage layers make MgF_2 a good choice for the ion conductor in EC devices. This reduction in switching voltage is a first step toward powering an EC device by an integrated semitransparent single-junction photovoltaic (PV) cell. In a side-by-side bench test, where the EC device is connected to a semitransparent *a*-SiC:H PV cell having on open circuit voltage of 0.87 V, a relative transmission change in the EC device of 40% is achieved in less than 60 s. © *1996 American Institute of Physics.* [S0021-8979(96)04714-7]

I. INTRODUCTION

Because of its excellent optical and physical properties, tungsten oxide (WO_3) is often the preferred material for electrochromic (EC) devices in which a change of coloration can be obtained by applying a small voltage. Since the initial work of Deb in the 1960s,[1] there have been enormous efforts to fabricate practical EC devices, and some small scale versions are now commercially available. Although there is still controversy about the detailed coloration mechanism of tungsten oxide, it is generally accepted that the injection and extraction of electrons and metal ions (Li^+, H^+,...) play a key role. In the case of lithium ions, this reaction can be written as[2]

$$WO_3 + xLi^+ + xe^- \leftrightarrow Li_xWO_3, \tag{1}$$

where WO_3 is colorless and Li_xWO_3 has an absorption band in the near infrared with a shoulder toward the visible range.[1] The ability to modulate its transmissivity by ion injection makes WO_3 well suited for ''smart-window'' applications, which can significantly reduce the cooling cost of buildings.[3] Designs for such EC devices have been described by many authors[4] and will be mentioned here only briefly. A typical EC device consists of a thin film of EC material (e.g., WO_3), an ion storage (IS) layer, and an ion conductor (IC) sandwiched between them. The IS layer allows the Li ions to be stored outside the EC layer when the device is in its bleached state. The IC layer conducts ions between the EC and IS layers but is electrically insulating. Usually, transparent conductors [e.g., indium tin oxide (ITO) or SnO] are deposited on each side of the whole stack as electrodes for delivery of the transmittance-modulating current.

Widespread application of EC cells depends on reducing cost and either increasing device lifetime or circumventing the problem of EC device degradation. The cost of EC windows has been estimated to range from \$100 to \$1000 /m^2,[5] which will itself hinder the large-scale application of this new technology. In addition, the installation of electrical wiring could add significant cost. By incorporating a photovoltaic (PV) power source into the EC window, however, this wiring cost could be reduced or eliminated, and the installation of the EC window could be greatly simplified. Furthermore, the acceptable lifetime of a retrofit, self-powered, PV–EC window might be shorter compared to a conventional EC window, because the former can be easily replaced.

Two possible PV–EC geometries have been considered. The first is a side-by-side geometry, in which part of the window is covered with solar cells; the second is a monolithic design, in which the EC layers are deposited on top of the PV layers. Of course, the second design requires a semitransparent PV device.[6,7]

Although the proof-of-concept for the monolithic design has already been demonstrated,[6,8] there are still many improvements needed, both for the EC and the PV cells, in order to fabricate a practical device. In this paper we will concentrate on physics crucial to the design of an EC device for the tandem PV–EC device and also present a first side-by-side PV–EC compatibility test. Some PV cell design issues were discussed in a previous paper.[9]

In a lithium-based EC device using an inorganic ion conductor the typical operating voltage is between 1.3 and 3 V,[10–12] but a single-junction *a*-SiC:H PV cell can only provide about 1 V. A two-junction PV cell could provide higher voltage output, but would be less transparent and more costly to produce. Therefore, for use in the tandem PV/EC design, we are developing an EC device that switches in a reasonable time at an operating voltage below 1 V. The switching speed is inversely proportional to the coloration current, I. Generally, the coloration current in an EC device can be expressed as

[a]Present address: Clemens Bechinger, Universitaet Konstanz, D-78434 Konstanz, Germany; Electronic mail: clemens.bechinger@uni-konstanz.de

 0021-8979/96/80(2)/1226/7/$10.00

$$I = V_e / R_t = [V_a - (\phi_{IS} - \phi_{EC}) - V_b]/R_t, \quad (2)$$

where V_e is the effective coloring voltage, V_a is the applied voltage, V_b is the sum of all interface barriers, and R_t is the sum of the resistances to electronic and ionic currents in the various layers. ϕ_{IS} and ϕ_{EC} are the internal chemical potential differences (emf's) of the IS and the EC layers, respectively. Recently it was pointed out that the difference between ϕ_{IS} and ϕ_{EC} is a fundamental factor determining the operating voltage of an EC device.[13] Of course, ϕ_{IS} and ϕ_{EC} are determined principally by the choice of IS and EC materials together with the choice of transporting ion. We have previously demonstrated theoretically that an EC device consisting of WO_3 and V_2O_5 as EC and IS layers should allow thermodynamic switching voltages well below 1 V.[14] However, reasonable switching speed can only be guaranteed by minimizing the interfacial barriers, V_b, and internal resistances, R_t, that determine I through Eq. (2).

In this paper, we report research aimed at development of a lithium-ion, all-solid-state electrochromic device with the structure of ITO/WO_3/MgF_2/V_2O_5/Au, for use in a monolithic PV–EC device. Here the MgF_2 layer is the ion conducting layer and V_2O_5 is the ion storage layer.[15–17] We deposit the devices on ITO-covered glass substrates to provide an electrical back contact. Semitransparent gold layers are used as top contacts to simplify fabrication. However, since Au layers reduce the transmission of the device and are not mechanically stable, they would be replaced in a commercial device with a second transparent conductor layer. Our device can be switched with voltages below 1 V and should meet our low-voltage requirements. The results of systematic-investigations of the internal interfaces of this device (WO_3/MgF_2, and V_2O_5/MgF_2) are presented to illustrate how the low switching voltage was obtained.

II. EXPERIMENT

ITO coated glass (12 Ω/□) was purchased from Donnelly Applied Thin Films Inc. for use as an electrically conductive, transparent substrate. Thin films of WO_3, MgF_2, and V_2O_5 were deposited by thermal evaporation of corresponding powders. Au layers were evaporated from a tungsten boat with gold pellets. The base pressure for the deposition process was normally about 10^{-5} mbar. The evaporation chamber was equipped with quartz lamps capable of heating the substrates as much as 200 °C.

The doping of the WO_3 films with Li was performed by thermal evaporation of pure Li metal onto the layer at a substrate temperature of $T_S = 120$ °C. Because lithium is highly reactive in air, we sealed it in the evaporation boat inside a glove box and opened it in the evaporation chamber under vacuum. The Li doping level was determined for a few samples by nuclear reaction analysis (NRA), yielding a correlation between doping values and the lithium deposition procedures with an accuracy of about ±10%. We did not perform NRA on all samples. Instead, we controlled the Li content using a quartz crystal monitor during Li deposition. Comparison between the crystal monitor reading and the NRA results enabled us to compute the tooling factor.

The ion mobility of Li was studied by means of alternating current (ac) impedance spectroscopy, using a Solatron model 1260/1265. An ac impedance spectrum is obtained by measuring the complex impedance as a function of the applied frequency, f, which varied in our experiments between 50 kHz and 0.005 Hz. The amplitude of the ac voltage is kept as small as possible to minimize disturbances to the system under investigation; in our case, the amplitude was 10 mV. While the high-frequency response is usually attributed to electronic properties of the sample, the low-frequency behavior can be ascribed to the response of ions to the applied ac electric field. The ac impedance technique is described in more detail elsewhere.[18] In addition to providing information about the ion resistivity, this technique also allowed us to study the transfer of lithium across the interfaces as a function of applied voltage.

The change in the optical transmittance of completed EC devices was monitored with a laser diode at 788 nm. Optical transmittance was recorded as a function of time after applying an external voltage with a computer-controlled potentiostat.

We tested the electrical compatibility of the PV and EC devices by placing independent PV and EC devices side by side under 1-sun illumination with external electrical connection. The active area of the EC device was 1 cm^2 and that of the semitransparent PV device was 0.5 cm^2. The white light transmission of the EC device was monitored with a short-circuited Si photodiode behind the EC device. The voltage supplied by the PV cell and the EC transmission were recorded as a function of time after closing the electrical connection.

A. Selection of the ion conductor

One of the most important points for the design of an EC device is the proper choice of the ion conductor, which must have a high ionic conductivity to reduce the switching time and a small electronic conductivity to decrease the self-discharge (self-bleaching) rate of the device. Furthermore, the resistance to ion transport between the ion conductor and the adjacent EC and IS layers must be minimized to keep the operating voltage low [see Eq. (2)]. Many IC materials have been prepared in the form of thin films, as reported in the literature.[19–22]

We selected MgF_2 as the ion conductor because MgF_2 single crystals are known to have a relatively high ionic conductivity for lithium,[23] as well as low electronic conductivity. Evaporated films, as used in this work, are known to form prismatic crystals with grain boundaries nearly parallel to the evaporation direction. Because of the loose packing of these columnar crystals [with a typical diameter of 10 nm (Ref. 24)], evaporated MgF_2 films have many pores and a large inner surface, which facilitates the diffusion of ions through the film and leads to a small value of R_t. Although these features suggest a good IC material, MgF_2 has only rarely been used as an IC in a Li-based EC device. Yoshimura *et al.*[25] reported fast switching times of about 200 ms for their Li-based EC devices, in which a 100-nm-thick evaporated MgF_2 film served as a combined ion conducting/storage layer. However, the permanent Li-storing sites in

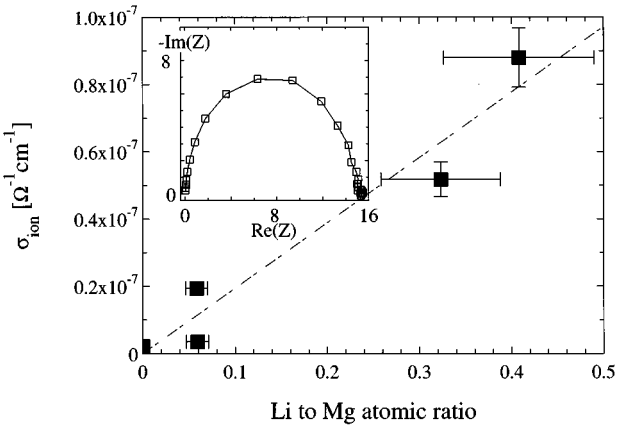

FIG. 1. Li^+ conductivity of evaporated MgF_2 films as a function of the Li to Mg atomic ratio. This ratio is estimated from the resonance frequency change of the crystal monitor during lithium deposition. The conductivity data were taken using ac impedance spectroscopy. A typical impedance spectrum is shown in the inset. The frequency at which the points are taken decreases from left to right. The extrapolation of the low-frequency branch to the real axis is used to measure the Li^+ conductivity.

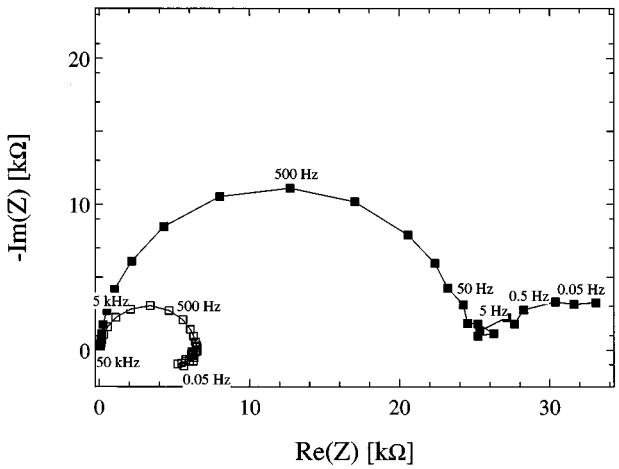

FIG. 2. ac impedance spectra for ITO/Li:WO_3/MgF_2/Au multilayer. The closed (open) symbols correspond to a negative (positive) bias applied to the WO_3 layer. The numbers correspond to the frequencies where the data were obtained.

MgF_2 (most likely, substitutional and Li on a Mg site that is compensated by a fluorine vacancy)[26,27] seemed to disappear after only a few hundred cycles, thereby reducing the Li ion storage efficiency. Thus, the ion storage capability of evaporated MgF_2 films was not sufficient for its use as an IS layer. This limitation, however, does not rule out its use as an ion conductor, as in the present study.

It is well known that deposition temperature is a critical parameter determining the properties of MgF_2 thin layers. Films deposited at room temperature are quite porous and incorporate considerable adsorbed water, making these films quite unstable.[24] However, when the deposition temperature is raised, the density of the films increases; they are less susceptible to water adsorption and much more stable in air.[28] Our MgF_2 films were, therefore, deposited at 120 °C.

III. RESULTS AND DISCUSSION

A. Li mobility in MgF_2

For Li ion mobility measurements, we deposited several MgF_2 films on ITO-coated substrates and doped the MgF_2 with different amounts of Li. From the resonance frequency change of the crystal monitor during the Li evaporation, we found that the Li to Mg atomic ratio varied from 0 to almost 0.5. The ion resistivity was then determined by ac impedance spectroscopy. The inset of Fig. 1 shows a Nyquist plot of a typical impedance spectrum. Here, the negative of the imaginary part of the impedance Z is plotted vs the real part of Z with the frequency f as a parameter. The frequency decreases from left to right along the curve. The roughly semicircular shape of the curve (which is also found in the case of crystalline material[27]) suggests that the Li-doped MgF_2 layer can be understood in terms of a simple parallel circuit consisting of a capacitor C and a resistor R. Deviations from a perfect semicircle can be caused by internal screening effects of the lithium ions. The ionic resistance, R_{ion}, can easily be obtained by extrapolation of the low-frequency branch to the real axis. We measured R_{ion} for several MgF_2 films doped with different amounts of Li. The corresponding ion conductivities (σ_{ion}) are plotted in Fig. 1 as a function of the Li-doping level. There is a monotonic increase of σ_{ion} with increasing lithium concentration, suggesting Li ions carry the dc current. The linear relationship is also in agreement with the corresponding results for Li-doped MgF_2 crystals.[27] For our MgF_2 films, the Li-ionic conductivity ranges between 10^{-8} and 10^{-7} $\Omega^{-1}\,\text{cm}^{-1}$, which should lead to reasonable coloration times for an EC device incorporating a MgF_2 IC layer.[22]

B. Interface ac impedance

The switching voltage of our EC device must be lower than 1 V if it is to be powered by a single-junction a-SiC:H PV cell. According to Eq. (2), we must, therefore, minimize interfacial voltages drops (resistance to Li ion migration) at the IC–EC and the IC–IS interfaces.

To study Li mobility across the WO_3/MgF_2 interface, we deposited 500 nm WO_3 on an ITO-coated substrate at a temperature of 120 °C. We then evaporated a nominal thickness of 30 nm Li. Finally, we evaporated 200 nm of MgF_2 at 120 °C and 50 nm of gold at room temperature. The gold film was used as a non-ion-injecting top electrode for ac impedance measurements.

Typical Nyquist plots that we measured for the Li-doped WO_3/MgF_2 sample are shown in Fig. 2. The closed symbols represent the impedance when the WO_3 layer is biased at -1 V. In this case, the external electric field drives the Li^+ ions into the tungsten oxide. At higher frequencies the curve follows a rough semicircle, as in the Li-doped MgF_2 films (see Fig. 1). Toward lower frequencies, however, the negative of the imaginary part (which is proportional to the internal damping) increases. This feature, usually ascribed to a diffusion-limited ion conduction process, is typical for Li in WO_3 films, and has been observed and analyzed in detail by other authors.[29] The diffusion limitation can be caused either

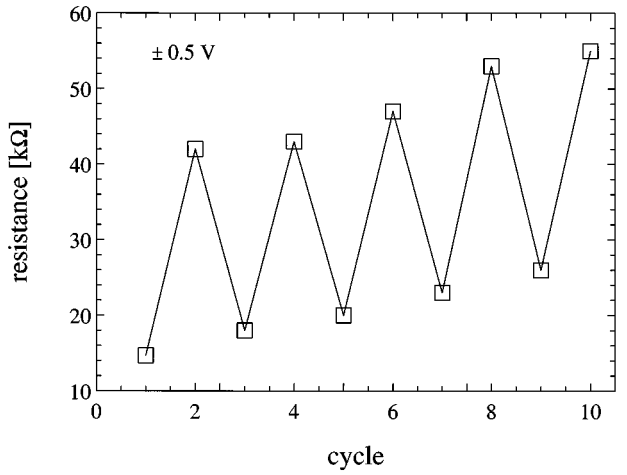

FIG. 3. Development of the steady-state ionic resistance of a ITO/Li:WO_3/MgF_2/Au multilayer structure as the applied bias voltage is cycled between ±0.5 V. The values for the resistance are obtained by extrapolation of the ac impedance spectra (e.g., Fig. 2) to the abscissa.

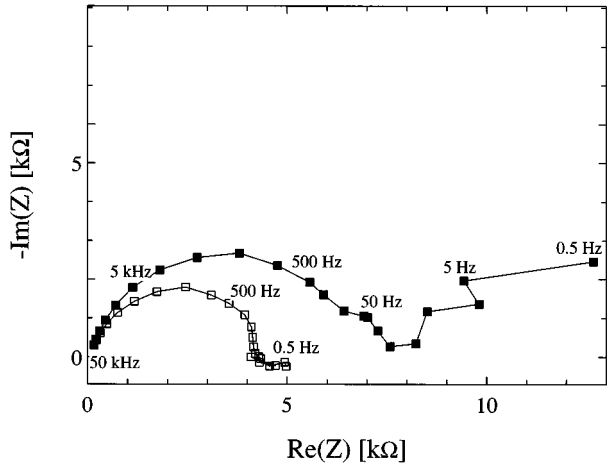

FIG. 4. ac impedance spectra for ITO/Li:V_2O_5/MgF_2/Au multilayer. The closed (open) symbols correspond to a negative (positive) bias applied to the V_2O_5 layer. The numbers correspond to the frequencies where the data were obtained.

by the coexistence of dissipative and storage phenomena in the material[30] or by pores at the interface between a solid electrolyte and a blocking metal electrode.[31] Both phenomena are likely to occur in our samples.

Reversing the bias voltage drives Li^+ ions into the MgF_2 and changes the ac impedance spectrum considerably (see Fig. 2, open symbols). The diameter of the semicircle, corresponding to R_{ion}, decreases by more than two thirds. Furthermore, the low-frequency response exhibits a behavior quite similar to the ac impedance spectrum of the Li-doped MgF_2 film on ITO (see Fig. 1). The Li ions are almost completely mobile in the MgF_2 and no damping (i.e., no increase in the imaginary part) occurs at low frequencies. We cycled the applied bias voltage several times from positive to negative and always observed spectra similar to those of Fig. 2.

Figure 3 shows the real-intercept values of the impedance spectra for several measurements where the applied bias was alternately $+0.5$ V and -0.5 V. It can be seen that even at these smaller voltages there is a large difference in the lithium mobility, depending on whether the WO_3 or the MgF_2 layer is biased to negative potential. When the ions are in the MgF_2, the ion conductivity is dramatically increased. This result strongly suggests that Li ions can be readily moved across the MgF_2–WO_3 interface with relatively small voltages.

Figure 3 also shows an upward trend of R_{ion} as a function of the cycle number. We assume that this is caused by irreversible reactions occurring over the course of the experiment. These may be related to the permanent trapping of lithium in MgF_2 discussed above.[25]

To study the Li mobility across the V_2O_5/MgF_2 interface, we first deposited 200 nm of V_2O_5 on an ITO-coated substrate and then 30 nm of Li, both at a temperature of 120 °C. Finally, 200 nm of MgF_2 at 120 °C and 50 nm of gold at room temperature were evaporated. Figure 4 shows the results of ac impedance spectroscopy of this structure with bias voltages of ±0.5 V. As in the case of the WO_3–MgF_2 device (Fig. 2), the ac impedance spectrum of the Li:V_2O_5–MgF_2 device changes dramatically upon reversing the applied bias voltage (Fig. 4). When the V_2O_5 is negatively biased, we again observe a diffusion–limited process at the lowest frequencies, which is reasonable for Li ions in this material. Reversing the voltage makes this part of the spectrum disappear and also reduces the ionic resistivity, indicating that Li^+ ions drifted across the interface and we are studying their conduction in MgF_2. Comparing Figs. 4 and 2 we see that the low frequency ionic resistivities are comparable in the two MgF_2 layers.

From these experiments we conclude that interface resistivities and interface barriers to ion migration are low at both the IC–EC and IC–IS interfaces. Any barriers to ion transport must be less than 0.5 V.

C. EC device characteristics

After these preliminary experiments, in which only parts of the device were tested, we fabricated complete all-solid-state EC cells (approximately 1 cm×1 cm) by sequential evaporation of WO_3, Li, MgF_2, V_2O_5, and a thin semitransparent Au electrode on top. The substrate temperature, T_S, was 120 °C for WO_3, Li, and MgF_2 deposition. T_S for Au deposition was room temperature. T_S during V_2O_5 evaporation was found to strongly affect the properties of the EC devices. We present results on devices where the V_2O_5 deposition temperature was room temperature (type A) or 75 °C (type B). The doping level, x, in the Li_xWO_3 films was determined with NRA to be $x=0.37$.

Figure 5 shows the optical and electrical response of a type A device as a function of time during a coloration and bleaching cycle at ±1 V. At −1 V (negative bias to the WO_3), the transmission of the device decreased, approaching its near-saturation value after 60 s. After the voltage was reversed, bleaching occurred in about 10 s, a much shorter time scale. The relative change of transmission was about 50%. Faughnan and Crandall[32] previously pointed out that coloring and bleaching (charge injection and extraction) are not completely symmetric phenomena. This asymmetry is

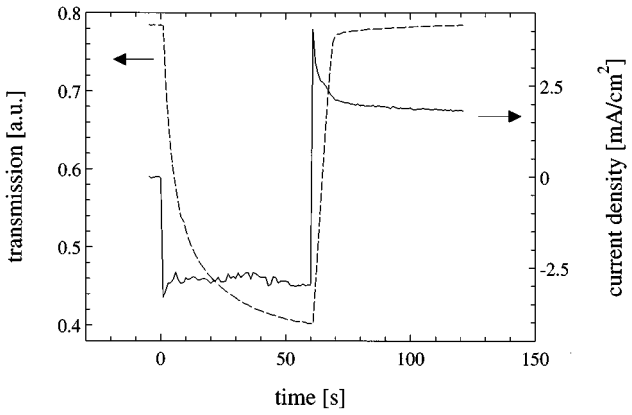

FIG. 5. Relative transmission (dashed) and current density (solid) of a 1 cm^2 all-solid-state Type A EC device during coloration and bleaching with ± 1 V. Each polarity is applied for 60 s. The relative change of transmission is about 50%.

also shown by the current density, which is somewhat higher during coloration than during bleaching (Fig. 5). During coloration, the total current flow is dominated by unintentional internal short circuits that carry about 2.5 mA/cm^2. Because Li injection takes place very slowly it perturbs the total current density during coloration very little. In contrast, immediately after reversing the voltage, a high bleaching current density decreases over about 30 s toward its limiting short-circuit value of about 2.4 mA/cm^2. Bleaching takes place on a shorter time scale than coloration and, therefore, requires a much higher initial current density than is carried by the internal short circuits.

The same experiments were also performed with type B devices, with results shown in Figure 6. As before, we applied ± 1 V to the cell, and this resulted in coloration and subsequent bleaching of the device (dashed line). With the type B device the transmission changes occurred on a somewhat longer time scale. This may result from denser type B V_2O_5 films that slow Li diffusion in this material. The saturation current density (solid line) is less than 0.01 mA/cm^2

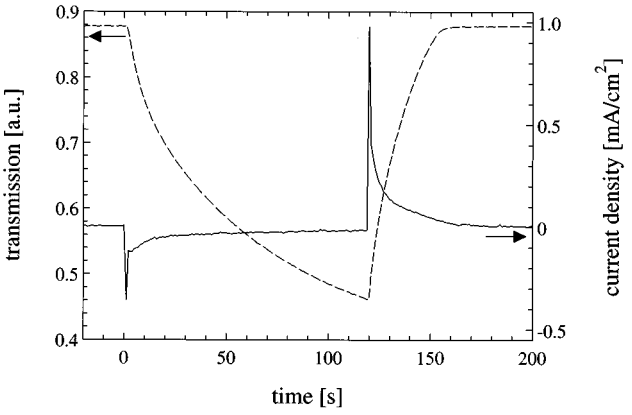

FIG. 6. Relative transmission (dashed) and current density (solid) of a 1 cm^2 all-solid-state Type B EC device during coloration and bleaching with ± 1 V. Note the dramatic reduction of saturation current density compared to Fig. 5. The relative change of transmission after 120 s is about 40%.

for both coloration and bleaching. This is a dramatic reduction compared to the Type A device of Fig. 5. The increased T_S during V_2O_5 deposition in type B samples greatly reduces the internal electrical shorting we observed in type A devices. Since we also observed a visible degradation after operating several type A devices (typically the V_2O_5 film appeared to be completely destroyed), we speculate that the short paths are formed by the reaction of Li with residual water in the V_2O_5 layer of type A devices. We believe a violent chemical reaction between residual adsorbed water and the deposited Li metal leads to local damage of the sample, and finally causes the observed electrical shorts. We have observed a similar phenomenon in tungsten oxide films evaporated at room temperature.

To check for degradation effects in this EC device, we cycled both type A and type B devices at ± 1 V in air and in an argon filled dry box. In air, we found almost no change in the optical behavior of the device after as many as 5000 cycles. For longer cycling in air, however, corrosion problems caused device failure. We assume this is due to a reaction of lithium with water that penetrates our unencapsulated devices. Cycling the device in an argon atmosphere decreased the depth of its optical switching. After about 100 cycles, the relative change of transmission decreased roughly to one half. When we cycled the device in air again, it recovered its original properties after a further 100 cycles. This behavior shows that our devices are somewhat moisture sensitive and suggests that mixed ionic conductivity (lithium and protons) may occur in moist environments. In practical devices the Au contact would be replaced with a much thicker ($\sim$400 nm) transparent conducting electrode that would also control the water content in the device. Because of the low switching voltage of the device, which is well below the ionization potential of water, our EC design should then provide considerable stability.

As previously mentioned, the requirements for our EC device are somewhat different from those of conventional EC devices. In order to power this device with a PV cell, the voltage amplitude for cycling the device between transparent and colored states should not exceed 1 V; otherwise, a more opaque two-junction *a*-Si PV cell would be required to provide the higher voltages. Therefore, both the coloration and the bleaching voltage must be kept as small as possible. In the course of experiments it turned out that both type A and type B devices are self-bleaching without any applied voltage (i.e., simply by shorting the top and bottom terminals). An example of this self-bleaching is shown in Fig. 7 for the type A device of Fig. 5. At $t=0$ the sample was colored with 1 V, leading once again to a decrease in the transmission. At $t=60$ s, the EC device was shorted by setting the potentiostat to 0 V. This shorting was sufficient to bleach the device, although the time scale was now much longer than that for -1 V bleaching (Fig. 5). It takes about 3 min (in the case of the type B device, 8 min) to reach the saturation transparency. This is fast enough for building-window applications.

D. PV–EC compatibility test

To test the electrical compatibility of our low-voltage EC devices with a semitransparent PV cell, we electrically

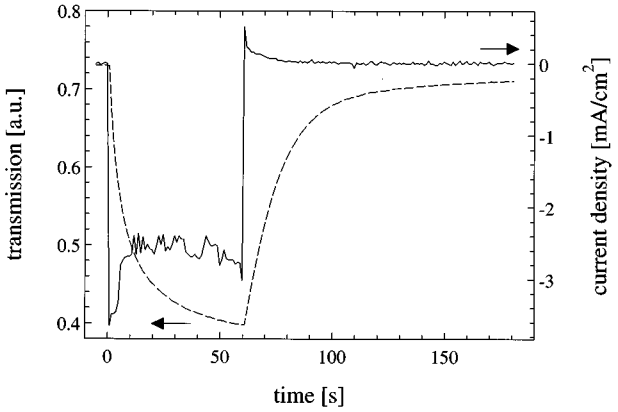

FIG. 7. Transmission (dashed) and current density (solid) of the same Type A device as in Fig. 5. Coloration is induced by applying −1 V for 60 s but bleaching is induced by simply shorting the device terminals (0 V applied).

connected one of our Type A EC devices (area 1 cm^2) to a single junction *a*-SiC:H PV device (area 0.5 cm^2) and placed them side-by-side. The open-circuit voltage of the PV was V_{oc}=0.87 V, the short-circuit current was J_{sc}~3.9 mA/cm^2, and the fill factor was 0.58. The semitransparent *a*-SiC:H PV cell used for this experiment is described in more detail in Ref. 9. Figure 8 shows the result of simultaneously measuring the white light transmission through the EC device (solid line) and the voltage supplied by the PV device (dashed line) after the leads are connected at t=0 s. When electrical connection is made, the EC device transmission drops within 60 s to about 40% of its bleached-state transmittance. Immediately after closing the electrical connection the voltage drops below 0.8 V since the EC coloration current flowing through the circuit is high. After about 60 s, when coloration is almost completed, the voltage reaches a steady-state value 0.02 V less than V_{oc}. This small difference from V_{oc} is due to electrical shorts in the type A EC device. This effect (and the PV current required for coloration) would be reduced by using the type B device. Later, when we short circuited the EC device, it spontaneously bleached within several minutes.

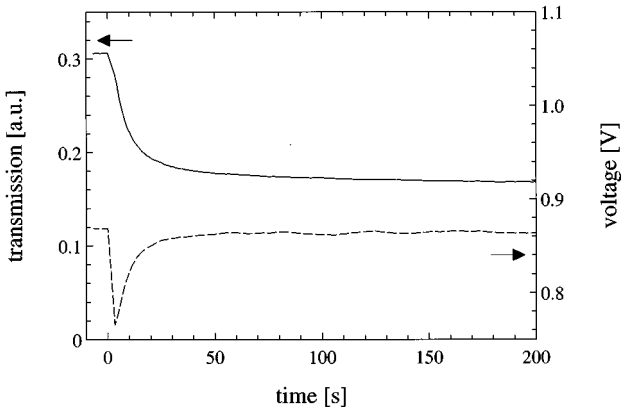

FIG. 8. White-light transmission through EC device (solid) and the switching voltage (dashed) supplied by an *a*-SiC:H PV cell under 1-sun illumination as a function of time.

IV. CONCLUSIONS

We investigated the optical and electrical properties of a novel solid-state EC device for PV-powered EC windows. The device structure was ITO/WO_3/MgF_2/V_2O_5/Au. The evaporated MgF_2 was a good choice of ion conductor because its lithium mobility (as measured by ac impedance spectroscopy) is high enough for our purposes. Further, we found any barriers to Li ion exchange between the MgF_2 layer and either the WO_3 and the V_2O_5 films are small. This small barrier was demonstrated with ITO/MgF_2/WO_3/Au and ITO/MgF_2/V_2O_5/Au test structures in which distinct changes in the impedance spectra are observed when the applied bias is switched between ±0.5 V.

The transmission and the current density of our devices were investigated during coloration and bleaching. We observed that relative changes of transmission up to about 50% in our devices (1 cm×1 cm) could be induced with a voltage of only −1 V, somewhat lower than that used in conventional devices. We also found that bleaching could be accomplished simply by shorting the device, which means that only one voltage polarity is required to operate such a device.

A side-by-side bench test of electrical compatibility between our EC device and a semitransparent a-SiC:H solar cell showed that we can achieve good coloration (40% relative transmission change) and reasonable switching speed with voltages well below 1 V. Upon shorting the EC device, bleaching occurred spontaneously within several minutes. We fully expect that a monolithic PV–EC device will function similarly.

ACKNOWLEDGMENTS

The authors wish to thank David Walsh at the Sandia National Laboratories for performing NRA measurements on our samples and Shyam Kocha of NREL for helpful discussions. Yueqin Xu skillfully assisted in the deposition of the PV cell. This work is supported by the U.S. Department of Energy, Advanced Energy Projects Office of Basic Energy Sciences. Clemens Bechinger's work is also supported by the Deutsche Forschungsgemeinschaft.

[1] S. K. Deb, Philos. Mag. **27**, 801 (1973).
[2] B. W. Faughnan, R. S. Crandall, and P. M. Heyman, RCA Rev. **36**, 176 (1975).
[3] W. A. Bartovics, M. S. thesis, MIT, 1984.
[4] S. E. Selkowitz and C. M. Lampert, in Large-Area Chromogenics: Materials and Devices for Transmittance Control, edited by C. M. Lampert and C. G. Granqvist; SPIE **IS4**, 22 (1988).
[5] C. M. Lampert, Sol. En. Mat. Sol. Cells **32**, 307 (1994).
[6] D. K. Benson and H. M. Branz, Sol. En. Mat. Sol. Cells **39**, 203 (1995).
[7] D. K. Benson and H. M. Branz, Proceedings of the First International Meeting on Electrochromism, Murano-Venice, Italy, October 1994, NREL/TP-452-7461.
[8] H. M. Branz, R. S. Crandall, and C. E. Tracy, U.S. Patent No. 5 377 037 (1994).
[9] J. N. Bullock, Y. Xu, D. Benson, and H. M. Branz, Mat. Res. Soc. Symp. Proc. **377**, 589 (1995).
[10] C. G. Granqvist, *Handbook of Inorganic Electrochromic Materials* (Elsevier, New York, 1995).
[11] R. B. Goldner, in *Solid State Ionic Devices*, edited by B. V. R. Chowdari and S. Radhakrishna (World Scientific, Singapore, 1988), pp. 379-390.
[12] S. F. Cogan and R. D. Rauh, U.S. Patent No. 5080471 (1992).

[13] R. D. Rauh and S. F. Cogan, J. Electrochem. Soc. **140**, 378 (1993).
[14] J. N. Bullock and H. M. Branz, Proc. SPIE **2531**, 152 (1995).
[15] S. F. Cogan, N. M. Nguyen, S. J. Perrotti, and R. D. Rauh, J. Appl. Phys. **66**, 1333 (1989).
[16] A. Talledo, A. M. Andersson, and C. G. Granqvist, J. Mater. Res. **5**, 1253 (1990).
[17] J.-G. Zhang, D. K. Benson, C. E. Tracy, S. K. Deb, A. W. Czanderna, and R. S. Crandall, J. Electrochem. Soc. **141**, 2795 (1994).
[18] D. D. Macdonald and M. C. H. McKubre, *Impedance Measurements in Electrochemical Systems* (Plenum, New York, 1982), Vol. 14.
[19] L. Zhang, M. Yahagi, and K. S. Goto, Solid State Ion. **18**, 1163 (1986).
[20] A. M. Glass, K. Nassau, and T. J. Negron, J. Appl. Phys. **49**, 4808 (1978).
[21] R. B. Goldner and T. E. Haas, *Annual Report of Research*, DOE Grant FG03-85SF15927 (January, 1991).
[22] DOE/SF/16733-F, final report, EIC Laboratories, (March, 1991).
[23] K. K. Kim and A. S. Nowick, J. Phys. C **10**, 509 (1977).
[24] H. K. Pulker and E. Jung, Thin Solid Films **9**, 57 (1971)
[25] T. Yoshimura, M. Watanabe, Y. Koike, K. Kiyota, and M. Tanaka, Jpn. J. Appl. Phys. **22**, 157 (1983).
[26] D. S. Park and A. S. Nowick, J. Phys. Chem. Solids **37**, 607 (1976).
[27] J. Toulouse, *Atom Transport in Li doped MgF_2 Crystals*, technical report, Grants DMR 77-07141 and 80-06326 (Columbia University Press, New York, 1981).
[28] CERAC Coating Material News **2** (1992).
[29] C. Bohnke and M. Rezrazi, Mater. Sci. Eng. B **10**, 313 (1991).
[30] J. Jacquelin, in 1st Electrochemical Impedance Spectroscopy Symposium, edited by C. Gabrielli, Bombannes, 1989, Extended Abstract C.26
[31] A. K. Jonscher, Electrochim. Acta **35**, 1595 (1990).
[32] B. W. Faughnan and R. S. Crandall, in *Display Devices*, edited by J. I. Pankove (Springer, Berlin, 1980), Chap. 5.